Sector-Based Encoding and Data Compression of Virtual Acoustic Scattering

Raimundo Gonzalez, Christoph Hold, Tapio Lokki
Dept. of Signal Processing and Acoustics
Aalto University
Espoo, Finland
{raimundo.gonzalezdiaz, christoph.hold, tapio.lokki}@aalto.fi

Archontis Politis
Audio Research Group
Tampere University
Tampere, Finland
archontis.politis@tuni.fi

***Abstract*—In order to produce high fidelity representations of sound-fields in spatial audio applications, the acoustical nuances occurring within physicals spaces must be included. This includes the effects of scattering from the boundary surfaces of enclosed spaces, as well as the scattering from finite bodies within spaces. Recently, a method has been proposed to encode the properties of arbitrary scattering geometries into the spherical harmonic domain in the form of a scattering expansion matrix. The following study extends this previous method by providing a sector-based approach. This approach allows for the encoding of selective regions of the scattering geometry, such as the upper hemisphere. Furthermore, a second optimization is also proposed to compress and reduce the memory storage of the scattering expansion matrix. Two methods for compression are proposed, with one of them providing minimal loss of fidelity by means of the Singular Value Decomposition.**

***Index Terms*—Virtual Acoustics,Scattering,Compression**

I. Introduction

Virtual acoustics is not only an active field of research, but also a growing industry due to its applications in room acoustic modelling as well as Virtual and Augmented Reality. Most of the research in the field of virtual acoustics has focused on modelling the acoustics of rooms either through ray-based [1] or wave-based approaches [2]. Another active field within virtual acoustics is the modelling of sound sources and receivers. Parametric methods for generating Head-related Transfer Functions (HRTFs) have been proposed [3], [4] as well as wave-based models for receivers [5]. Furthermore, sound sources and their directivity have been modeled through spherical harmonic (SH) decomposition [6] and finite-difference or finite-element methods [7], [8].

A less active area, yet still important, is modeling the effects of scattering for virtual acoustic purposes. We refer to scattering as the effects of reflection, occlusion and/or diffraction contributed to the acoustic field by some body. Scattering is important for listening environments because it can affect the perception of the acoustic spaces [9]. The effects of scattering from walls and large boundaries have been implemented in ray-tracing frameworks using scattering coefficients [10]. Still, inconsistencies between methods to produce scattering coefficients and the lack of modeling diffraction produces audible deviations in room color as well as in source localization [11]. Still, not much work exists for the efficient rendering of scattering of finite bodies within virtual sound-fields.

Recently, a method to encode the scattering properties of arbitrary geometries into the spherical harmonic domain has been proposed [12]. A spherical harmonic representation of scattering benefits from the existing efficient platforms for rendering spherical harmonics signals, such as High-Order Ambisonics [13], as well as its various manipulation tools: rotation, translation and scaling. A downside to this method, is that it requires a data set of the scattered pressure surrounding the geometry for an entire sphere. This is an inconvenient requirement considering we might be interested in a limited scattering region of the geometry, for example an object on the floor or wall, and simulating acoustic data can be computationally expensive to produce at high frequencies. Previous attempts exist for encoding the sound pressure of a limited spherical sector [14], [15]. Yet, some of these methods make use of basis functions which are not entirely spherical [14] and not directly compatible with Ambisonics. Furthermore, the proposed scattering expansion matrix is frequency dependent and can be quite large, taking fair amount of memory space. For example, the full scattering expansion matrix for 48 frequencies between 100 Hz and 5 kHz for an object inscribed within a 50 cm radius sphere, can take up to 3.4 GB. In this paper we propose a method to encode selected regions of scattering arbitrary geometries in order to minimize the amount of data required to encode the scattering into the spherical domain, as methods to reduce the storage of these matrices in memory.

II. Scattering model

A total field p_t produced by a scattering body in the path of an incident plane wave can be defined via the superposition of:

$$p_t = p_i + p_s \tag{1}$$

where p_i describes the incident field produced by some source and p_s is the outgoing scattered field radiated from the scattering body. By inscribing the scattering body inside the volume of a sphere of radius R, as presented in Figure 1, we can define the scattered field p_s beyond R as an exterior problem [16]. Making no assumptions on the shape of the object,

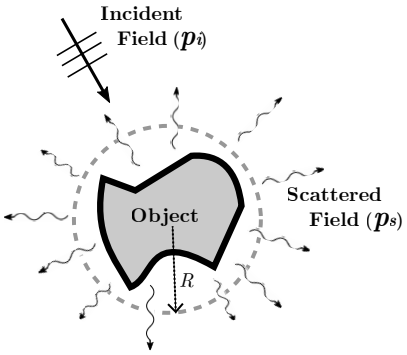

Fig. 1: Scattering scene

the scattered sound field pressure $p_s(f, \tilde{\mathbf{x}}_i, \mathbf{x}_j)$ at distance $r = ||\mathbf{x}_j|| \geq R$ from the center of the sphere and direction $\tilde{\mathbf{x}}_j$, due to a unit amplitude plane wave impinging from a direction of arrival $\tilde{\mathbf{x}}_i$, is given by:

$$p_s(f, \tilde{\mathbf{x}}_i, \mathbf{x}_j) = \sum_{n=0}^{\infty} \sum_{m=-n}^{n} C_{mn}(f, \tilde{\mathbf{x}}_i)\ h_n^{(2)}(kr)\ Y_n^m(\tilde{\mathbf{x}}_j) \quad (2)$$

where $k = 2\pi f/c$ is the wavenumber for a frequency f, $h_n^{(2)}$ is the outgoing Hankel function, and Y_n^m is a real spherical harmonic of order n and degree m. C_{nm} denote modal scattering expansion coefficients that are dependent on frequency and incident direction $\tilde{\mathbf{x}}_i$.

If the continuous scattered pressure over the surface of the surrounding sphere is known, the scattering expansion coefficients C_{mn} can be obtained by the spherical harmonic transform (SHT) of that pressure:

$$C_{nm}(kR, \tilde{\mathbf{x}}_i) = \frac{1}{h_n^{(2)}(kR)} \int_{\tilde{\mathbf{x}} \in S^2} p_s(kR, \tilde{\mathbf{x}}_i, \tilde{\mathbf{x}})\ Y_n^m(\tilde{\mathbf{x}})\ \mathrm{d}A(\tilde{\mathbf{x}}) \quad (3)$$

where $\mathrm{d}A(\tilde{\mathbf{x}})$ is the spherical surface differential element $\mathrm{d}A(\tilde{\mathbf{x}}) = \cos\theta \mathrm{d}\theta\mathrm{d}\phi$. Note that compared to the preceding formulas the frequency dependency is now integrated into the more representative wavenumber-distance product kR.

In practice, the infinite series of the scattered pressure in Equation (2) is truncated to a maximum order N with negligible error if $N \geq kR$ [13], [17]. Additionally, the C_{nm} scattering expansion coefficients can be recovered through a discrete SHT by a grid $\mathbf{X}_J = [\mathbf{x}_1, ..., \mathbf{x}_J]$ of regularly distributed scattered pressure samples $\mathbf{p}_s = [p_1, ..., p_J]^T$ over the surface of the sphere, where $J \geq (N+1)^2$ and $N \geq kR$. This process can be expressed in a compact form as:

$$\mathbf{c}(kR, \tilde{\mathbf{x}}_i) = \frac{4\pi}{J} \mathbf{D}^{-1}(kR)\ \mathbf{Y}(\tilde{\mathbf{X}}_J)\ \mathbf{p}_s(f, \tilde{\mathbf{x}}_i, \mathbf{X}_J) \quad (4)$$

where $\mathbf{D}$ is a $(N+1)^2 \times (N+1)^2$ diagonal matrix whose entries are the radial Hankel functions, $\mathbf{y}(\tilde{\mathbf{x}}) = [Y_0^0(\tilde{\mathbf{x}}), ..., Y_N^N(\tilde{\mathbf{x}})]^T$ is a $(N+1)^2$ vector of SH values up to order N, and $\mathbf{Y}(\tilde{\mathbf{X}}_J) = [\mathbf{y}(\tilde{\mathbf{x}}_1), ..., \mathbf{y}(\tilde{\mathbf{x}}_J)]$ is a $(N+1)^2 \times J$ matrix of SH values for the grid directions $\tilde{\mathbf{X}}_J$. Note that, respectively, the coefficient vector $\mathbf{c}$ contains all the coefficients C_{nm} up to order N.

Furthermore, if $\mathbf{c}$ is known for I regularly distributed incident plane wave directions, we can construct a matrix $\mathbf{C}(kR, \tilde{\mathbf{X}}_I) = [\mathbf{c}(\tilde{\mathbf{x}}_1), ..., \mathbf{c}(\tilde{\mathbf{x}}_I)]$ of size $(N+1)^2 \times\ I$ that contains all the coefficients for the I directions. Subsequently, a discrete SHT can be applied along the incident sphere of directions of the $\mathbf{C}$ matrix as:

$$\mathbf{S}(kR) = \frac{4\pi}{I}\ \mathbf{C}(kR, \tilde{\mathbf{X}}_I)\ \mathbf{Y}(\tilde{\mathbf{X}}_I)^T. \quad (5)$$

The resulting $(N+1)^2 \times (N+1)^2$ matrix $\mathbf{S}$ expresses the scattering of the object as a MIMO system [18] between spherical modes of the incident field and spherical modes of the radiating scattered field. It gives a continuous spatially band-limited expression of the scattering at arbitrary directions. Finally, the scattered pressure field at point $\mathbf{x}_j$ outside of $R < ||\mathbf{x}_j||$ can be expressed by:

$$p_s(f, \tilde{\mathbf{x}}, \mathbf{x}_j) = \mathbf{y}(\tilde{\mathbf{x}}_j)^T\ \mathbf{D}(kr)\ \mathbf{S}(kR)\ \mathbf{y}(\tilde{\mathbf{x}}_i). \quad (6)$$

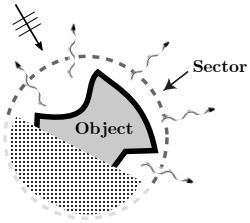

Fig. 2: Sector region

III. Sector-Based Encoding

Consider a discrete description of the scattered pressure for a limited sector over the surface of a sphere, as presented in Figure 2. The objective is to recover a scattering expansion matrix $\hat{\mathbf{S}}$ which accurately describes only the regions of the sphere for which information is provided. The discrete SHT as in Eq. (4) and (5) demands quadrature weights, which are constant only for regular grids. These weights are not easily found for potentially incomplete grids, such as in Figure 2 or the upper hemisphere evaluated later. Instead, we can pose the encoding to the spherical harmonic domain as a system of linear equations for which a least squares solution for $\hat{\mathbf{c}}$ minimizes the energy of the residual

$$\arg\min_{\hat{\mathbf{c}}} ||\mathbf{D}\mathbf{Y}\hat{\mathbf{c}} - \mathbf{p}_s||_2 \quad (7)$$

where $||\cdot||_2$ denotes the l_2 vector norm and the superscript $\hat{}$ indicates the scattering expansion coefficients for a limited sector of a sphere. The least-square solution is given by

$$\mathbf{Y}^\dagger = (\mathbf{Y}^T\mathbf{Y})^{-1}\mathbf{Y}^T \quad (8)$$

and therefore the direction-dependent scattering coefficients can be recovered through

$$\hat{\mathbf{c}}(kR, \tilde{\mathbf{x}}_a) = \frac{4\pi}{B} \mathbf{D}^{-1}(kR)\ \mathbf{Y}^\dagger(\tilde{\mathbf{X}}_B)\ \mathbf{p}_s(f, \tilde{\mathbf{x}}_a, \mathbf{X}_B) \quad (9)$$

where a and b are the indices for A and B which describe the directions for a sector of the sphere. A and B can be a subset

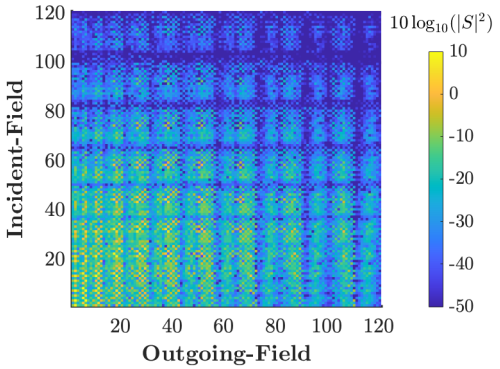

Fig. 3: Energy of scattering expansion matrix for a body enclosed by 0.5 m sphere at 1kHz in decibel scale.

of a full spherical set of directions I and J used in Section II. Now considering that we have a similar limited description for the incident field directions of the scattered field, the same process can be applied and a sector-based scattering expansion matrix can be recovered by

$$\hat{\mathbf{S}}(kR) = \frac{4\pi}{A}\, \hat{\mathbf{C}}(kR, \tilde{\mathbf{X}}_A)\; \mathbf{Y}^{\dagger}(\tilde{\mathbf{X}}_A)^T. \tag{10}$$

IV. Data Compression

The SH order required to model the scattering expansion matrix with low error can be determined by the $N \geq kR$ rule. This indicates that storage requirements can be determined per modeled frequency point f_i, with $N_i = 2\pi f_i R/c$. Such a scheme, for example, modeling a scattering body enclosed in an 0.5 m sphere at a maximum frequency of 1 kHz would require an order of about $N = 10$ and a scattering expansion matrix of size $11^2 \times 11^2$, as seen in Figure 3. At lower frequencies the order, and size of the scattering expansion matrix, will be decreasing, down to a single scalar coefficient of order $N = 0$ at DC. In this section we propose two approaches to compress and reduce the memory requirements of a scattering expansion matrix.

A. Energy-based Compression

The storage requirements of the $N = kR$ rule may still be too high for most practical applications, and they do not consider either the distribution of energy in the scattering coefficients due to the actual geometry of the scattering object, or the limited domain of possible incidence and/or radiation that depends on the geometry and application.

An aggressive compression can be achieved with a simple energy based rule. Since the energy in the scattering expansion matrix decreases towards the higher-order coefficients, a maximum truncation order $N' < N$ can be determined based on the cumulative energy up to order N' with respect to the total energy, captured in the diagonal of $\mathbf{S}$

$$E(N') = \sum_{q=1}^{(N'+1)^2} |[\mathbf{S}(kR)]_{qq}|^2. \tag{11}$$

The ratio $E(N')/E(N)$ can then be used to determine N' based on a threshold $\gamma_E < 1$,

$$\arg\max_{N'} E(N') \quad \text{s.t.} \; \frac{E(N')}{E(N)} < \gamma_E. \tag{12}$$

It is expected that lower energy thresholds will achieve higher compression at the expense of a higher reconstruction error.

B. SVD-based Compression

The symmetrical properties of the scattering expansion matrix will depend on the symmetry of the scattered field which then depends on the symmetry of its scattering body. Making no assumptions on the symmetry of the scattering object we assume that $\mathbf{S}$ might not be symmetric. Still, we expect $\mathbf{S}$ to exhibit some internal structure, i. e. not *spatially white*. This leads to the idea of decomposing, and ultimately compressing, the scattering expansion matrix based on its Singular Value Decomposition (SVD). The complex valued matrix $\mathbf{S}$ can be expressed as $\mathbf{S} = \mathbf{U}\mathbf{\Sigma}\mathbf{V}^*$, where $\mathbf{U}$ and $\mathbf{V}$ are unitary matrices, and $\mathbf{\Sigma}$ a diagonal matrix holding the real, non-negative singular-values. Sorting the singular-values and corresponding entries in $\mathbf{U}$ and $\mathbf{V}$ allows to determine the contribution of each component to $\mathbf{S}$. We define the cumulative sum of the singular-value up to an order N' as:

$$G(N') = \sum_{q=1}^{(N'+1)^2} \Sigma_q \tag{13}$$

and the ratio $G(N')/G(N)$ can then be used to determine N' based on a threshold $\gamma_{SVD} < 1$,

$$\arg\max_{N'} G(N') \quad \text{s.t.} \; \frac{G(N')}{G(N)} < \gamma_{SVD}. \tag{14}$$

Truncating the singular-values to a threshold of γ_{SVD}, the matrix dimensions of $\mathbf{U}, \mathbf{\Sigma}, \mathbf{V}$, leads to the truncated representation

$$\underline{\mathbf{S}}_{SVD}(kR) = \underline{\mathbf{U}}\,\underline{\mathbf{\Sigma}}\,\underline{\mathbf{V}}^* = \underline{\mathbf{U}}\,\underline{\mathbf{T}} \quad . \tag{15}$$

If storing the full $n \times n$ square matrix $\mathbf{S}$ needs n^2 elements, then storing the un-truncated SVD needs $2n^2 + n$ elements. We may rewrite with $\underline{\mathbf{T}} = \underline{\mathbf{\Sigma}}\,\underline{\mathbf{V}}^*$, which only requires storing two matrices. When truncating to $\tilde{n}$ single values, storing the corresponding matrices $\underline{\mathbf{U}}, \underline{\mathbf{T}}$ demands storing $2n\tilde{n}$ elements. Comparing leads to the amortization point of $\tilde{n} = n/2$, hence compression gain occurs beyond smaller $\tilde{n}$. As motivated earlier, the scattering expansion matrix is typically not *spatially white*, which means that the eigenvalues in $\mathbf{\Sigma}$ will decrease. Therefore, we expect the truncation based on the SVD to result in less reconstruction error than the energy-based compression, when comparing similar order truncation.

V. Evaluation

As a case study for the proposed method, the scattered field for a limited region of a complex geometry was simulated using the Boundary-Element Method (BEM) module of COMSOL Multiphysics [19]. The simulated geometry, as shown in Figure 4a, is a $80 \times 50 \times 3$ cm rectangle with

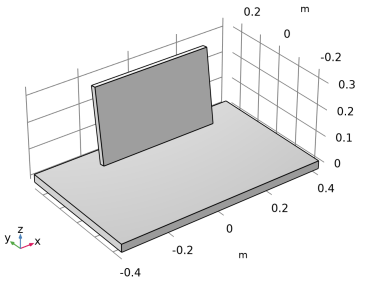

(a) 3D model used for acoustic simulations.

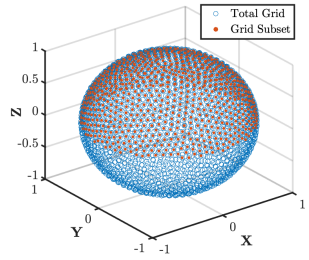

(b) Total sampling grid (2116 points) and grid subset (1062 points)

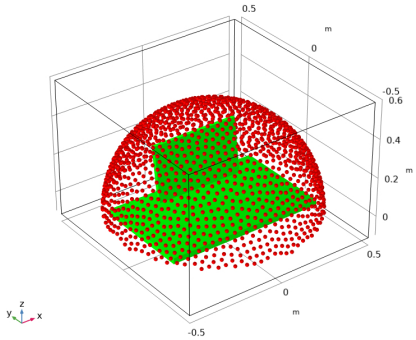

(c) Sampling grid of 1062 points over the surface of a hemisphere

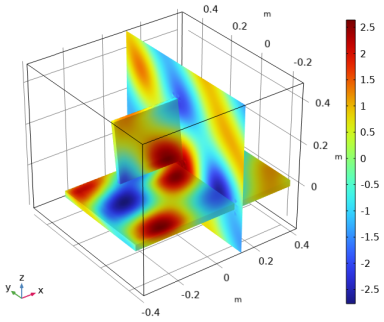

(d) Total pressure over surface of geometry and cross sectional area along y-axis, for an incident 1 kHz plane wave incoming from 0° azimuth and 30° elevation.

Fig. 4: Modelling case study, a desk with a monitor.

another $45 \times 28 \times 2$ cm rectangle rotated 99° degrees along the x-axis. This model intends to represent the geometry of a work desk which includes some form of computer screen. The acoustic scattering of this geometry is relevant for room acoustic simulations were several workstations maybe present in a room, as well as virtual reality applications were subjects are performing tasks near their virtual workstations. In both of these mentioned scenarios, the acoustic contributions of interest to the total field, comes from the scattering of the upper hemisphere of the geometry.

Following the required constraints, the spherical grid selected for the acoustic simulation made use of a subset containing 1062 points of the 2116 points from a 45^{th} order maximum determinant grid (compare Figure 4b). The maximum determinant grid [20] is a *critical* sampling grid, i. e. with the minimum number of points $J = (N+1)^2$, as to achieve minimal memory requirements. The grid could be determined for very high spherical orders with well behaved sampling weights, which makes them appropriate as a spherical quadrature to carry out the (least-squares) SHT in Eq. (10). The new hemispherical sampling grid was scaled to 50 cm, 2 cm beyond the furthest bounds of the geometry, as shown in Figure 4c, in order to meet the exterior boundary value conditions from Eq. (2).

The incident field used for the simulation was far-field plane-waves following the 1062 incident directions, for 48 frequencies from 104 Hz to 5 kHz. Figure 4d presents a visualization of the total pressure field, incident and scattered, for a single planewave over surface of the geometry. The scattering sound pressure around the geometry was then sampled for the same 1062 directions and the incident field was removed from the final scattered sound field. For the meshing in the BEM simulation, a free quadrilateral mesh was used with a spatial resolution of $\frac{1}{6}$ of the wavelength of the simulated frequency [19]. The scattering coefficients C_{nm} for each incident direction were recovered using Eq. (9) and then organized as a matrix $\mathbf{C}$ to recover the scattering expansion matrix $\hat{\mathbf{S}}$ through Eq. (10). The matrix $\hat{S}$ was then compressed using the two methods proposed in the Section IV. For the energy-based approach, the matrix $\underline{\mathbf{S}}_E$ was truncated per frequency at $\gamma_E = 0.9\%$. For the SVD-based approach, $\underline{\mathbf{S}}_{SVD}$ was compressed using various parameters. First, the matrix was compressed for the same frequency-dependent truncation orders as the energy-based method at $\gamma_E = 0.9\%$, which allows to compare both methods in terms of error performance. Then, $\underline{\mathbf{S}}_{SVD}$ was compressed for γ_{SVD} thresholds of 0.9 and 0.99. The recovered matrix $\mathbf{S}_{SVD}$, as well as its various compressed versions were then used to synthesize the scattered pressure at same 1062 sampling positions for original 1062 incident directions. Figure 5 presents the root-mean-square error (RMSE) between the initial scattered pressure used for the encoding process and the scattered pressure synthesized from the sector based encoded matrix as well as its compressed iterations.

VI. Discussion

As indicated in Figure 5, the sector-based encoding approach $\hat{\mathbf{S}}$ produces minimal error between reference and synthesized scattered pressures. For the remaining compressed cases, the RMSE varies. The direct removal of scattering expansion components in the energy-based compression approach in $\underline{\mathbf{S}}_E$ considerably reduces the storage of the matrix

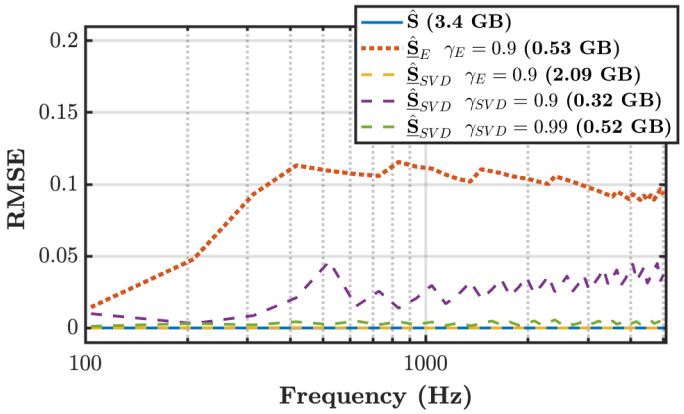

Fig. 5: RMSE between reference and synthesized scattered pressure for many sampling and incident directions, for uncompressed and compressed scattering expansion matrices

to 16% of its original size, but it also introduces the largest error from all cases. For the SVD-based compressed matrices $\underline{\mathbf{S}}_{SVD}$, the amount of error depends on the order at which singular-values are truncated. The truncation of singular-values using the same orders as the those determined in the energy-based method produces minimal error although the matrix is compressed only by 61% of its original size. This is due to the drawback of storing two matrices instead of only one. In the case where the SVD-based truncation is applied according to the normalized cumulative sum of its singular-values, a $\gamma_{SVD} = 0.9$ threshold reduces the matrix to 9% of its original size while introducing noticeable error. This shows that a similar truncation criterion for the SVD-based approach, compared to the energy-based approach, results in greater compression gain and still less error. A good compromise is found at a threshold of $\gamma_{SVD} = 0.99$ where the matrix is compressed to 15% of its original size at the cost of very small error. The latter compromise was chosen such that the resulting compression gain between both approaches is similar, which reveals superior error performance of the SVD-based approach. In fairness, this last compression threshold value might be specific to this particular geometry and geometries with more complex scattering patterns might require higher compression thresholds.

VII. Conclusions

A method is proposed for encoding the scattering of limited regions of geometries for virtual acoustic applications. The incomplete description of the pressure over the spherical surface of the scatterer is posed as a least-squares problem. Furthermore, a lossless compression method is proposed for the purposes of storing encoded scattering. A study case is presented with a geometry relevant for spatial audio applications and the implementations of both methods reveal minimal error between reference and synthesized cases. The proposed methods provide flexibility for the implementations of arbitrary scatterers within spatial audio environments.

References

[1] L. Savioja and U. P. Svensson, "Overview of geometrical room acoustic modeling techniques," *The Journal of the Acoustical Society of America*, vol. 138, no. 2, pp. 708–730, 2015.

[2] S. Bilbao, "Modeling of complex geometries and boundary conditions in finite difference/finite volume time domain room acoustics simulation," *IEEE Transactions on Audio, Speech, and Language Processing*, vol. 21, no. 7, pp. 1524–1533, 2013.

[3] R. Duda and W. Martens, "Range-dependence of the HRTF for a spherical head," in *Proc. IEEE Workshop on Applications of Signal Processing to Audio and Acoustics*, Mohonk, New Paltz, NY, 1997.

[4] G. Ramos and M. Cobos, "Parametric head-related transfer function modeling and interpolation for cost-efficient binaural sound applications," *J. Acoust. Soc. Am.*, vol. 134, no. 3, pp. 1735–1738, 2013.

[5] S. Bilbao, A. Politis, and B. Hamilton, "Local time-domain spherical harmonic spatial encoding for wave-based acoustic simulation," *IEEE Signal Processing Letters*, vol. 26, pp. 617–621, 2019.

[6] M. Noisternig, F. Zotter, and B. Katz, "Reconstructing sound source directivity in virtual acoustic environments," in *Principles and Applications of Spatial Hearing*. World Scientific, 2011, pp. 357–372.

[7] S. Bilbao and J. Ahrens, "Modeling continuous source distributions in wave-based virtual acoustics," *J. Acoust. Soc. Am.*, vol. 148, no. 6, pp. 3951–3962, 2020.

[8] D. L. James, J. Barbič, and P. K. Dinesh, "Precomputed acoustic transfer: output-sensitive, accurate sound generation for geometrically complex vibration sources," *ACM Transactions on Graphics (TOG)*, vol. 25, no. 3, pp. 987–995, 2006.

[9] L. Shtrepi, A. Astolfi, G. D'Antonio, and M. Guski, "Objective and perceptual evaluation of distance-dependent scattered sound effects in a small variable-acoustics hall," *J. Acoust. Soc. Am.*, vol. 140, no. 5, pp. 3651–3662, 2016.

[10] Y. W. Lam, "A comparison of three diffuse reflection modeling methods used in room acoustics computer models," *J. Acoust. Soc. Am.*, vol. 100, no. 4, pp. 2181–2192, 1996.

[11] F. Brinkmann, L. Aspöck, D. Ackermann, S. Lepa, M. Vorländer, and S. Weinzierl, "A round robin on room acoustical simulation and auralization," *J. Acoust. Soc. Am.*, vol. 145, no. 4, pp. 2746–2760, 2019.

[12] R. Gonzalez, A. Politis, and T. Lokki, "Spherical decomposition of arbitrary scattering geometries for virtual acoustic environments," in *Proc. 23rd Int. Conf. on Digital Audio Effects (DAFx-20)*, 2021.

[13] S. Moreau, J. Daniel, and S. Bertet, "3D sound field recording with higher order ambisonics - objective measurements and validation of a 4th order spherical microphone," in *Proc. 120th Convention of the AES*, 2006, pp. 20–23.

[14] D. Kumari and L. Kumar, "Spherical sector harmonics representation of sound fields using a microphone array over spherical sector," *J. Acoust. Soc. Am.*, vol. 149, no. 1, pp. 145–157, 2021.

[15] H. Sun, S. Yan, and U. P. Svensson, "Optimal higher order ambisonics encoding with predefined constraints," *IEEE Transactions on Audio, Speech, and Language Processing*, vol. 20, no. 3, pp. 742–754, 2012.

[16] E. G. Williams, *Fourier Acoustics*. Cambridge, MA: Academic Press, 1999.

[17] D. B. Ward and T. D. Abhayapala, "Reproduction of a plane-wave sound field using an array of loudspeakers," *IEEE Transactions on Speech and Audio Processing*, vol. 9, no. 6, pp. 697–707, 2001.

[18] H. Morgenstern, B. Rafaely, and M. Noisternig, "Design framework for spherical microphone and loudspeaker arrays in a multiple-input multiple-output system," *The Journal of the Acoustical Society of America*, vol. 141, pp. 2024–2038, 2017.

[19] C. Multiphysics, "Acoustics module user's guide," pp. 140–154, 2020. [Online]. Available: www.comsol.com/acoustics-module

[20] I. H. Sloan and R. S. Womersley, "Extremal systems of points and numerical integration on the sphere," *Advances in Computational Mathematics*, vol. 21, no. 1-2, pp. 107–125, 2004.